Renewable Energy 115 (2018): 226-237

DOI: https://doi.org/10.1016/j.renene.2017.08.062

Application of a non-noble Fe-N-C catalyst for oxygen reduction reaction in an alkaline direct ethanol fuel cell.

Luigi Osmieri [a,b] *, Ricardo Escudero-Cid [b] *, Alessandro H.A. Monteverde Videla [a], Pilar Ocón [b], Stefania Specchia [a]

[a] Politecnico di Torino, Dipartimento di Scienza Applicata e Tecnologia, Corso Duca degli Abruzzi 24, 10129, Torino, Italy.

[b] Universidad Autónoma de Madrid, Departamento de Química Física Aplicada, C/Francisco Tomás y Valiente 7, 28049, Madrid, Spain.

* Corresponding Authors:

luigi.osmieri@polito.it, ligiosmi@gmail.com;

ricardo.escudero@uam.es

Abstract

A Fe-N-C non-noble metal (NNM) catalyst for oxygen reduction reaction (ORR) catalyst was prepared via hard templating method using Fe(II)-phthalocyanine. Its electrochemical behavior towards the ORR was tested in alkaline conditions using cyclic voltammetry (CV) and rotating disk electrode (RDE) techniques. The kinetics of the reduction of the adsorbed oxygen, the selectivity, and the activity towards hydrogen peroxide reduction reaction (HPRR), were investigated. The ethanol tolerance and the stability in alkaline conditions were also assessed with the purpose to verify the good potentiality of this catalyst to be used in an alkaline direct ethanol fuel cell (DEFC). The results evidence that the ORR occurs mainly following the direct 4 e^- reduction to OH^-, and that the-Fe-N-C catalysts is highly ethanol tolerant with a promising stability. The alkaline DEFC tests, performed after the optimization of the ionomer amount used for the preparation of the catalyst ink, show good results at low-intermediate currents, with a maximum power density of 62 mW cm^{-2}. The initial DEFC performance can be partially recovered after a purge-drying procedure.

Keywords

Fe(II)phthalocyanine; rotating disk electrode; anion exchange membrane fuel cell; stability; hydrogen peroxide reduction; cyclic voltammetry.

1. Introduction

Polymer electrolyte membrane fuel cells (PEMFC) are devices which can directly convert the chemical energy of a fuel into electrical energy by means of electrochemical reactions [1]. PEMFC are particularly interesting for automotive application and portable power units since they operate at low temperatures, close to ambient conditions [2].

The fuels suitable to feed a PEMFC can be H_2 or low molecular weight organic molecules (such as methanol, ethanol, glycerol, or dimethyl ether) [3–6]. In particular, direct alcohol fuel cells (DAFC) are suitable for portable and off-grid applications, as they use liquid fuels. Compared to H_2, liquid fuels have higher energy density, and do not face the problems of fuel storage and transportation [7,8]. Therefore, DAFC can potentially compete with Li-ion batteries as power devices for small portable applications, with the additional advantage to be completely independent of the electric grid, since they can generate electricity continuously as long as the source of fuel is available and fed [9].

One of the main problems of PEMFC is the slow kinetics of the oxygen reduction reaction (ORR), which requires the use of noble metals (mainly Pt) as catalysts, with a consequent rise of the fabrication costs [10]. For DAFC, the electro-oxidation of the organic molecules occurring at the anode is a kinetically slow process as well, requiring the use of noble-metal based catalysts also at the anode [11].

PEMFC (and DAFC more in particular) can operate in two different configurations, depending on the properties of the membrane electrolyte: acidic configuration if the membrane is a protonic conductor, and alkaline configuration if the membrane is a conductor of OH^- ions [12].

The alkaline configuration for DAFC is advantageous for the kinetics of both alcohol oxidation reactions (especially if OH^- ions are fed in the alcohol solution) and ORR [13]. Among the different types of DAFC, direct ethanol fuel cells (DEFC) are of interest because they use ethanol as fuel, which is non-toxic and can be produced from biomass fermentation as a totally renewable source of energy [14].

To overcome the problem of the use of Pt as cathodic catalyst for PEMFC, the research has focused on the development of non-noble metal (NNM) catalysts for ORR [15]. The most promising materials reported in the literature in terms of ORR activity are carbonaceous materials doped with nitrogen and transition metals (Me-N-C, where Me = Fe, Co, Mn) synthesized using a wide range of approaches [16]. These materials have shown considerably higher ORR activity in alkaline than in acidic conditions [17], remarking the advantage of operating PEMFC in alkaline configuration from the catalysis point of view. In addition, compared to Pt-based catalysts, these Me-N-C materials possess a great tolerance to the presence of alcohols (high ORR selectivity), being consequently very interesting to be used at DAFC cathodes to reduce the detrimental crossover effect [18].

Among others, one of the possible synthesis methods of NNM is the use of a sacrificial template agent (*e.g.*, an ordered mesoporous silica) and an organic molecule containing Fe, N, and C as a unique source of the catalyst precursor. The catalyst is obtained after a pyrolysis process and subsequent removal of the sacrificial template [19–22].

In this work, our purpose was double. First, we wanted to complete the electrochemical characterization of the Fe-N-C catalyst in alkaline conditions, which was already partially presented (together with its physicochemical characterization) in a previous work [20]. Thus, we carried out some additional tests which are not usually reported in other literature studies on ORR catalysts in alkaline conditions, investigating the reduction of the adsorbed O_2 via cyclic voltammetry, the activity towards hydrogen peroxide reduction reaction (HPRR), the ORR activity in the presence of ethanol, and the durability and stability in RDE.

The second purpose was to demonstrate the applicability of the Fe-N-C as a cathodic catalyst in an alkaline DAFC. In fact, so far, the application of Me-N-C catalysts in DAFC cathodic material has been much less investigated compared to H_2-fueled PEMFC [18], especially in alkaline conditions. We carried out a preliminary optimization of the catalyst layer in terms of ionomer (Nafion®) content, and we investigated the short-term durability and stability of the DEFC device, which, to the best of our knowledge has been reported so far in the literature only in a work recently published by our group [12].

2. Experimental

2.1. Chemicals

Tetraethyl orthosilicate (TEOS, ≥ 98% purity), hydrochloric acid (HCl, 37 wt. %), Pluronic P123® triblock copolymer, hydrofluoric acid (HF, ≥ 40 wt. %), potassium hydroxide (KOH, 99.0% purity), ethanol (≥ 99.8% purity), acetone (≥ 99.8% purity), isopropanol (≥ 99.7% purity), Nafion® 5 wt. % hydroalcoholic solution, and iron(II) phthalocyanine $C_{32}H_{16}N_8Fe$ (Fe-Pc, 90% purity) were purchased from Sigma-Aldrich. Nitrogen and oxygen gases were supplied in cylinders by Air Liquide with 99.999% purity. Ultrapure deionized water (Millipore Milli-Q, with resistivity >18 MΩ cm) was used for the catalyst synthesis and the preparation of the solutions used in RDE tests. 20 wt. % Pt/C (HiSPEC™ 3000, Pt 20 wt. % on carbon black, Johnson Matthey), 40 wt. % Pt/C (HiSPEC™ 4000, Pt 40 wt. % on carbon black, Johnson Matthey) and 45 wt. % PtRu/C (HiSPEC™ 7000, Pt-Ru 45 wt. % on carbon black, Pt:Ru atomic ratio = 1, Johnson Matthey) were purchased from Alfa Aesar. Polybenzimidazole (PBI) membrane with 50 μm thickness was purchased from Danish Power Systems.

2.2. Synthesis of Fe-N-C catalyst and physicochemical characterization.

The Fe-N-C catalyst was synthesized following the procedure described in our previous works [22,23]. Briefly, 500 mg of Fe(II)-phthalocyanine was dissolved in a hydroalcoholic solution and wet-impregnated on 500 mg of SBA-15 silica. Then the solvent was evaporated under heating, and

the recovered powder was heat-treated for 1 hour at 800 °C under N_2 atmosphere. The SBA-15 silica was subsequently removed by washing with 5 % HF solution.

The results of the physicochemical characterization of the Fe-N-C catalyst are shown in other works of our group [22,23]. The main catalyst features are here briefly resumed: BET specific surface area = 1508 $m^2 g^{-1}$; micropores content = 48% of the BET surface area; bulk Fe content (by EDX) = 0.64 atomic %; surface Fe content (by XPS) = 0.1 atomic %; surface N content (by XPS) = 5.0 atomic %; the relative atomic % of the different types of N are: 12.5% nitrile-N, 26.9% pyridinic-N, 2.0% Fe-Nx moieties, 41.6% graphitic-N, 17.0% oxidized-N (by deconvolution of the XPS N 1s peak).

2.3. RDE measurements

For testing the Fe-N-C catalyst in the RDE, the ink was prepared by mixing 10 mg of catalyst powder with 150 µL of H_2O, 305 µL of isopropanol and 45.8 µL of Nafion® 5 wt. % solution. With this formulation, the Nafion-to-catalyst mass ratio (NCR) is 0.2. The ink was sonicated until a good dispersion was achieved. An amount of ink necessary to have a catalyst loading of 637 µg cm^{-2} was micropipetted on the glassy carbon surface of the RDE.

As a comparison, a Pt catalyst (20 wt. % Pt/C) was also tested. In this case, the ink was prepared by dispersing 10 mg of catalyst (considering the total mass of Pt and C), 20 µL of deionized water, 33 µL of 5 wt% Nafion® solution and 734 µL of isopropanol. The ink was ultrasonicated until good dispersion, and an amount corresponding to a Pt loading of 38 µg cm^{-2}, was pipetted on the RDE electrode.

The electrochemical tests were performed in a three-electrodes cell, using an RDE setup (PINE, USA) and a potentiostat/galvanostat (AutoPG, Spain). The cell was equipped with a glassy carbon disk working electrode (5 mm diameter), a graphite rod counter electrode, and a saturated Ag/AgCl reference electrode. The electrolyte was a 0.1 M KOH solution, saturated with N_2 or O_2 by direct bubbling the gas into the solution. Before start tests, 50 cyclic voltammetry (CV) cycles between

1.2 and 0.0 V vs RHE at 100 mV s^{-1} scan rate were performed in the N_2 saturated electrolyte to electrochemically clean the electrode surface.

For testing the electro-reduction of the adsorbed oxygen on the Fe-N-C catalyst, two CV cycles at different scan rates (200 – 100 – 50 – 20 – 10 mV s^{-1}) were recorded in N_2 and subsequently in O_2 saturated electrolyte from 1.2 to 0.0 V vs RHE. Between each CV experiment at different scan rate in the O_2-saturated electrolyte, gaseous O_2 was bubbled into the solution for 10 minutes, to allow O_2 adsorbing onto the catalyst surface.

Linear sweep voltammetry (LSV) at different RDE rotation speeds (200 – 500 – 900 – 1600 – 2400 – 3600 rpm) were recorded at 5 mV s^{-1} from 1.2 to 0.0 V vs RHE in the O_2-saturated electrolyte. To eliminate the capacitive current contribution, an LSV in N_2-saturated electrolyte was recorded in the same conditions, and subtracted from the LSV measured in O_2-saturated electrolyte.

The activity of the Fe-N-C catalyst toward the hydrogen peroxide electro-reduction reaction (HPRR) in absence of O_2 was tested performing LSV at 5 mV s^{-1} at different RDE speeds (200 – 500 – 900 – 1600 – 2400 – 3600 rpm) in N_2-saturated 0.001 M H_2O_2 + 0.1 M KOH solution from 0.9 to 0.0 V vs RHE.

The tolerance of the Fe-N-C catalyst to the presence of ethanol was assessed by recording LSV at 5 mV s^{-1} and 1600 rpm in an O_2-saturated 0.1 M KOH solution with different ethanol concentrations ranging from 0.001 M to 2 M. As a comparison, the same test was conducted for the commercial 20 wt. % Pt/C catalyst (in this case the LSV were recorded in both anodic and cathodic scan directions).

All the RDE measurements were performed at 25 °C and atmospheric pressure, and the electrode potentials were referred to the reversible hydrogen electrode (RHE). The current densities were normalized to the geometric area of the glassy carbon disk electrode.

To check the stability and durability of the Fe-N-C catalyst, two different tests were performed. The first test consisted in cycling the electrode potential for 10,000 times between 0.6 and 1.0 V vs. RHE under O_2-saturated electrolyte. An LSV at 5 mV s^{-1} and 1600 rpm was recorded at the

beginning of the test, and then after 400, 4,000 and 10,000 cycles. The second test consisted in a chronoamperometry conducted during 48 hours at a constant potential of 0.765 V vs RHE.

2.4. Alkaline DEFC test

Fe-N-C was tested as ORR catalyst in a single alkaline DEFC. The cell active area was 2.89 cm^2. A commercial PBI membrane doped with OH^- ions was used as a polymeric electrolyte. To induce the anionic conductivity, the PBI membrane was treated for 7 days with a 6 M KOH solution. After this treatment, the ionic conductivity of the membrane reached a value of ~ 0.01 S cm^{-1} [24]. A commercial Pt-Ru/C catalyst (45 wt% Pt-Ru, Pt:Ru 1:1) was used as anodic catalyst, and the anode of the DEFC was prepared with a Pt-Ru loading of 2 mg cm^{-2} and a Nafion® content on dry electrode of 4 wt. %, as optimized in a previous work [22].

The Fe-N-C cathode was prepared by spraying the catalyst ink with an airbrush onto a gas diffusion layer (ELAT GDL-LT 1200 W). The ink was prepared by mixing the catalyst powder with an isopropanol/deionized water solution (2:1 vol.) and an adequate amount of Nafion® ionomer solution (5 wt. %). The quantity of Nafion® solution was in accordance with the desired amount of ionomer in the dry catalytic layer. Electrodes with a Fe-N-C catalyst loading of 2.5 mg cm^{-2} and a Nafion® content of 4, 35, and 50 wt. %, respectively, were prepared.

As a comparison, the performance of an alkaline DEFC prepared using a commercial Pt/C catalyst (40 wt. % Pt) at the cathode was also evaluated. The Pt loading was 1 mg cm^{-2} and the Nafion® content on the dry electrode was 4 wt. % [25].

The electrodes and the membrane were assembled without hot pressing, by direct sandwiching at room temperature in the cell hardware [26].

A fuel cell test bench (MITS Pro-FCTS, Arbin Instruments, USA) was used to record the polarization curves. The DEFC anodic compartment was fed with 2 M ethanol + 2 M KOH solution preheated at 80 °C with a flow rate of 1 mL min^{-1} and a pressure of 0.33 bar (relative). The cathodic compartment was fed with 200 NmL min^{-1} pure O_2 preheated at 80 °C, with a backpressure of 3 bar

and no humidification. The cell temperature was 90 °C. The polarization curves were recorded at 10 mV s^{-1} from open circuit potential (E_{oc}) down to 0.01 V.

3. Results and discussion

3.1. RDE measurements.

3.1.1. Reduction of adsorbed oxygen.

The behavior of the Fe-N-C catalyst towards the reduction of the adsorbed O_2 was investigated using cyclic voltammetry (CV). In a first test (see **Figure 1**), the CV measured in deaerated solution was subtracted from the CV measured in O_2-saturated solution. **Figure 1a** shows the CVs recorded at 10 mV s^{-1} under O_2-saturated (first and second consecutive cycles) and N_2-saturated solution, and the differential curves after the subtraction, which represent the current density peaks due to the faradic process (reduction of oxygen), free from pure capacitive and pseudo-capacitive contributions [27,28]. These faradic current peaks are due to the sum of the contribution of the reduction of the O_2 already adsorbed on the catalyst surface (when O_2 was left bubbling inside the solution) before the CV scan was started, and the O_2 diffusing from the bulk of the solution to the catalyst surface during the CV scan. If we compare the first differential curve in **Figure 1a** (CV in N_2-saturated solution subtracted from the first CV cycle in O_2-saturated solution) with the second one (CV in N_2-saturated solution subtracted from the second CV cycle in O_2-saturated solution) we notice that in the former, the current density peak is considerably higher than in the latter. In facts, in the former the contribution of the adsorbed O_2 reduction is higher, while in the former there is much more contribution of the diffused O_2 reduction.

Figure 1b shows the differential CVs calculated from the subtraction of the CV in N_2-saturated solution subtracted from the first CV cycle in O_2-saturated solution (that is, the ones where the contribution of the reduction of the adsorbed O_2 is higher) at different scan rates, with an evident increase of the intensity of the current density peak (I_p) and decrease of the peak potential (E_p) with

the increase of the scan rate (v). The contribution of the reduction of diffusing O_2 should be higher at lower scan rates.

According to the theory of the potentiodynamic technique, I_p increases proportionally to the square root of the scan rate ($v^{1/2}$) in the case of a diffusion-controlled process [29], and proportionally to v in the case of a process involving only adsorbed species [30,31]. In the I_p vs. $v^{1/2}$ plot in **Figure 1c**, a linear trend is observed, confirming that the contribution of the reduction of diffused O_2 cannot be neglected.

The ORR on Fe-N-C catalyst is an irreversible process, in facts, no reverse oxidation peak is observed in the CV plot in **Figures 1a-b**, and E_p is shifted towards lower potentials with the increase of v. Thus, it is possible to determine the cathodic transfer coefficient (α_c) from the plot of E_p vs. the logarithm of v. Assuming to be under the conditions of reaction of adsorbed species (with a negligible contribution of the reaction of diffused species), α_c can be calculated from the slope of the plot in **Figure 1d** using Equation (1) [32]:

$$\alpha_c = -\frac{2.3RT}{\text{Slope} \cdot F} \quad (1)$$

We obtained a slope of 171 mV, which corresponds to a value of $\alpha_c = 0.35$. In a similar study conducted in alkaline electrolyte on an ORR catalyst prepared using Fe, N, and C precursors, the α_c value obtained was 0.50 [33].

On the contrary, if we assume to be under the conditions of a diffusion-controlled process [32], α_c is given by Equation (2):

$$\alpha_c = -\frac{2.3RT}{\text{Slope} \cdot 2F} \quad (2)$$

and the corresponding α_c value is 0.17.

However, looking at the E_p vs. log(ν) plot in **Figure 1d**, the linear trend is not so good, and it seems that the slope is changing with the potential. Thus, we can divide the plot into two different zones, finding a better linear trend, with different slopes (and different α_c). This could indicate a change in the ORR reaction mechanism with overpotential. The first zone corresponds approximately to the

potential range 0.80 – 0.70 V vs. RHE, showing a α_c value of 0.23. The second zone corresponds approximately to the potential range 0.70 – 0.55 V vs. RHE shows a α_c value of 0.13.

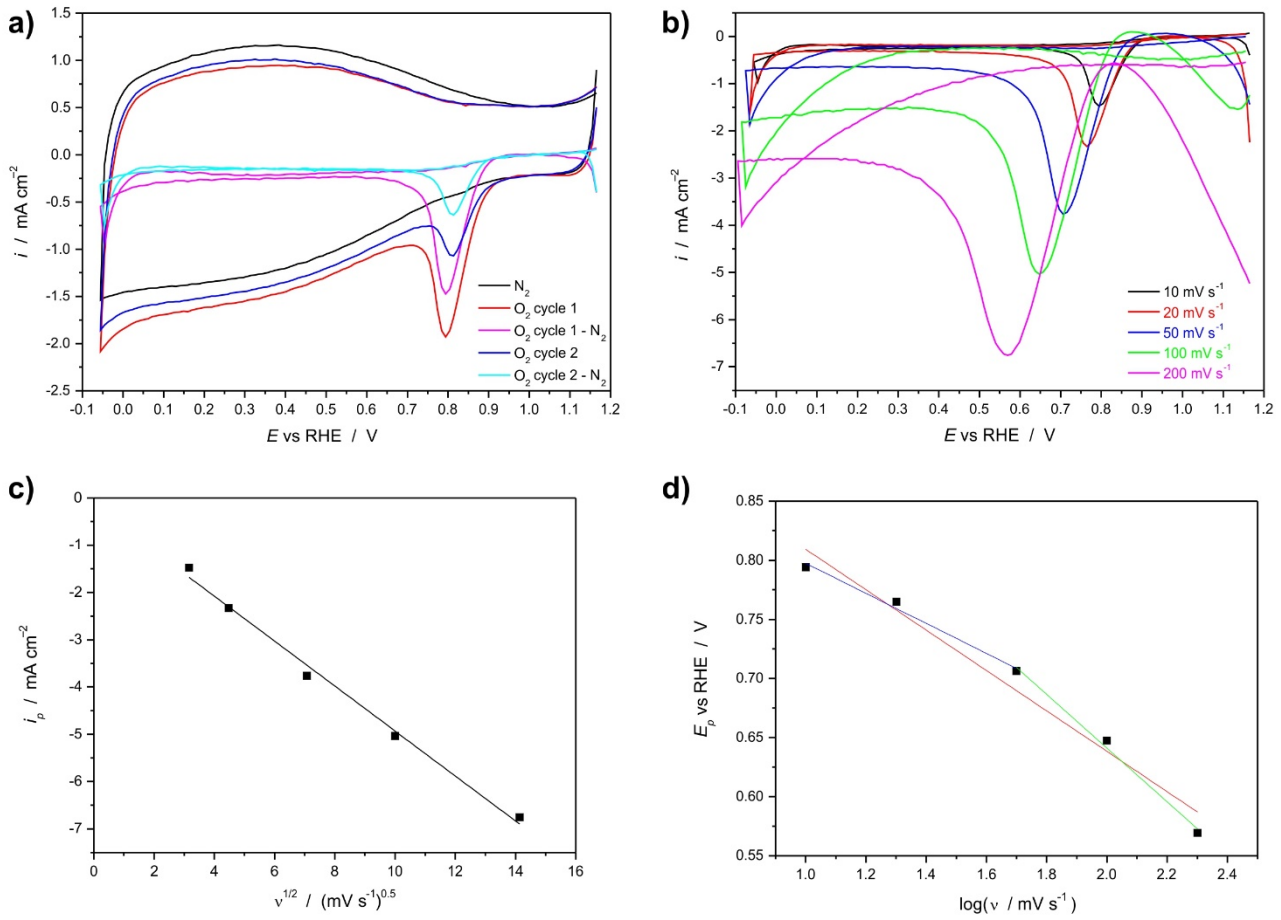

Fig. 1. (a) First cycle (red) and second cycle (blue) of the CV recorded at 10 mV s^{-1} in 0.1 M KOH solution saturated with O_2, CV cycle recorded in the same conditions in N_2-saturated solution (black), and the differential CV obtained after subtraction of the first cycle (magenta) and the second cycle (light blue). (b) Differential CV recorded at different scan rates. (c) I_p of the differential CV vs. square root of the scan rate. (d) E_p of the differential CV vs. logarithm of the scan sate.

In a second test, we recorded two consecutive CV cycles in O_2 saturated electrolyte, and we subtracted the second cycle from the first cycle, obtaining a differential voltammogram. Here, the contribution of the reduction of the diffused O_2 was eliminated (or reduced as much as possible), and the I_p measured can be ascribed almost totally to the reduction of the O_2 adsorbed on the catalyst surface before the potential scanning was started [31]. **Figure 2a** shows the differential voltammograms measured at different scan rates. The peaks are fully developed and almost

247 symmetrical for all of the scan rates examined, and the I_p values are approximately in the range 1 –
248 6 mA cm^{-2}. From the full width at half maximum ($\Delta E_{1/2}$) of the differential peaks, according to the
249 theory of the potential sweep voltammograms in the case of diffusionless systems [30], it is possible
250 to calculate α_c using Equation (3):
251 $\alpha_c = 62.5 \text{ mV} / \Delta E_{1/2}$ (3)
252 On the other hand, considering a process totally governed by diffusion, from the value of the
253 difference between the peak potential (E_p) and the potential corresponding to half the peak current
254 on the ascending portion of the voltammogram ($E_{p/2}$), it is possible to calculate α_c using Equation
255 (4) [29]:
256 $\alpha_c = 48 \text{ mV} / |E_p - E_{p/2}|$ (4)
257 **Figure 2b** shows the variation of α_c with E_p calculated with both methods described above. A
258 decrease of α_c with the decrease of E_p (which decreases with the scan rate) is observed. The α_c
259 values are close to unity at high E_p (low scan rate). This confirms what we found for the same Fe-N-
260 C catalyst in a previous work [23], where we measured α_c from the Tafel slope from a static
261 polarization curve recorded in RDE experiment in alkaline conditions: there, we found an α_c value
262 of 0.94 in the potential range between 0.98 and 0.85 V vs RHE [23]. Curiously, this value ranges in
263 between the values calculated from the differential voltammograms with both Equations (3) and (4)
264 (see **Figure 2b**). Then, increasing the scan rate, the E_p value decreases, and a decrease of α_c at
265 lower values (between 0.6 and 0.2) is observed. These findings suggest a change in ORR
266 mechanism occurring with the variation of the potential. A similar trend of change in α_c was
267 observed in an acidic medium in another literature study [31], and also by our group (work under
268 preparation).

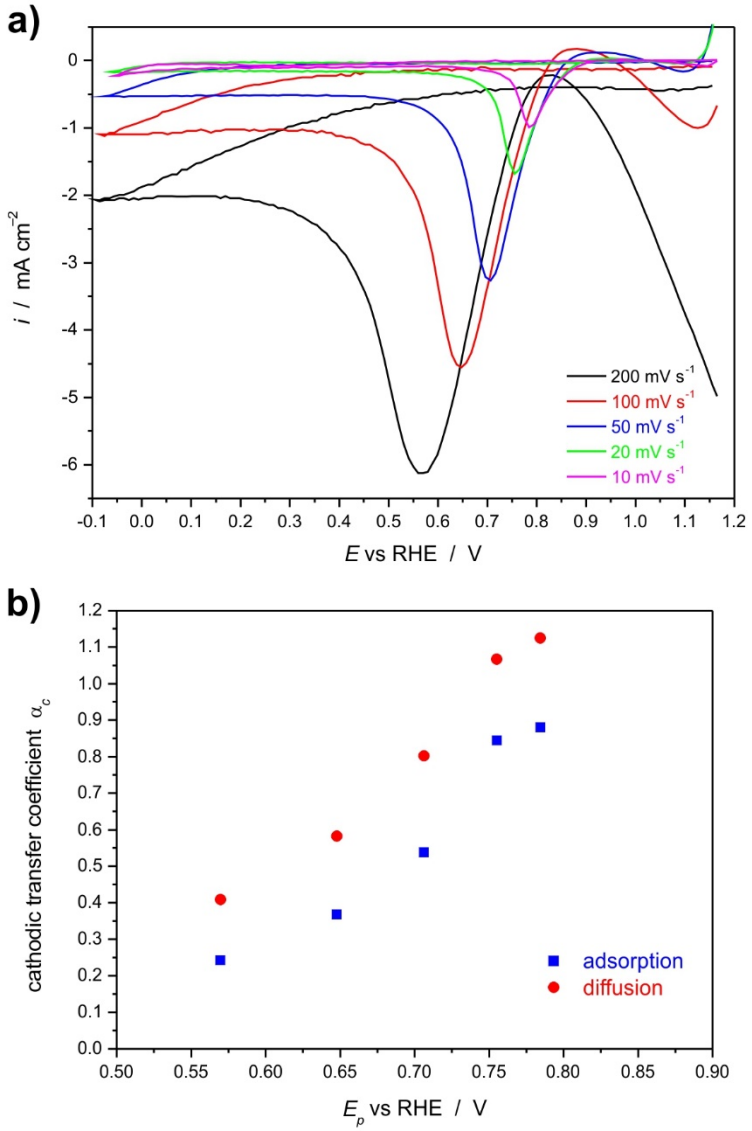

Fig. 2. (a) Differential CV recorded in O_2-saturated 0.5 M H_2SO_4 at different scan rates; (b) cathodic transfer coefficient for the reduction of O_2 in case of pure adsorption and pure diffusion.

3.1.2. Oxygen reduction vs. hydrogen peroxide reduction.

To investigate more in detail the ORR pathway on the Fe-N-C catalyst in alkaline conditions, we measured the polarization curves in O_2-saturated 0.1 M KOH at different RDE rotation speeds. **Figure 3a** shows the obtained results, evidencing that the ORR is under diffusional control for potentials lower than ~0.7 V vs. RHE for all the rotation speeds. An evident increase of the current density with the RDE speed is also observed. Considering the findings of our previous work [23], where we detected an almost null amount of HO_2^- ion (the stable form of H_2O_2 at high pH values)

280 in the rotating ring-disk electrode (RRDE) test, we can deduce that O_2 is mainly converted to OH^-
281 via a complete 4 e^- reduction on our Fe-N-C catalyst in alkaline medium.
282 In this work, we did not calculate the electron transfer number using the Koutecky-Levich (K–L)
283 method, because with the high catalyst loading used in the RDE experiment, the hypothesis of the
284 thin-film smooth electrode of the K–L theory are most likely not satisfied. In particular, the
285 peroxide intermediates produced were found to be autocatalytically decomposed as a function of
286 catalyst layer thickness [34]. Another reason of misinterpretation of kinetic data could come form
287 nano-particle modified rotating disk electrodes of partially covered and non-planar geometry [35].
288 In addition, as demonstrated and discussed in detail, among others, by R. Zhou et al.[36], the K–L
289 method is mainly inapplicable to ORR because this reaction is not a one-step first order reversible
290 reaction.
291 Considering that a complete 4 e^- reduction of O_2 to OH^- can be attained via a direct one-step 4 e^-
292 mechanism, via a two-step 2 e^- + 2 e^- mechanism, or via a combination of these, we performed a
293 further test to investigate more in depth the ORR pathway. We recorded the LSV polarization
294 curves in 0.1 M KOH at different rotation speeds, in the absence of oxygen (thus, saturating the
295 solution with N_2), and in the presence of H_2O_2 in the concentration of 1 mM, which is similar to the
296 concentration of O_2 in an aqueous solution saturated with O_2 at 25 °C. With this test, we measured
297 the activity of the Fe-N-C catalyst toward the HPRR. From the results in **Figure 3eb**, we can
298 deduce that HPRR currents increase with the cathodic overpotential almost linearly in the potential
299 range 0.8 – 0.5 V vs RHE. However, even at lower potentials, the current density never reaches a
300 plateau region, which is typical for processes controlled by diffusion (as was found for ORR in
301 **Figure 3a**). This happens for all the rotation speeds considered, thus no linear trend of current vs.
302 the square root of rotation speed can be found at any potential. Therefore, we can conclude that on
303 our Fe-N-C catalyst, the HPRR in alkaline conditions is under mixed kinetic-diffusional control on
304 all the potential range considered. Moreover, in spite of the same concentration of reactants in the
305 electrolyte solution (O_2 for ORR, and H_2O_2 for HPRR), the current densities measured for HPRR

306 are always considerably lower than the current densities measured for ORR. All these results let us
307 deduce that on this Fe-N-C catalyst the HPRR kinetics is much more sluggish than the ORR
308 kinetics. Together with the results of RRDE presented in our previous work [23], we can conclude
309 that the direct one-step 4 e^- reduction of O_2 to OH^- is the main reaction pathway on the Fe-N-C
310 catalyst in alkaline medium. The indirect 2 e^- + 2 e^- mechanism is occurring in an only negligible
311 amount, even less than as found in another work of our group for the same Fe-N-C catalyst in acidic
312 conditions [22].
313 The LSV at different rpm in **Figure 3a** show a broad current peak in the potential region 0.5 – 0.7 V
314 vs. RHE. This phenomenon has not been analyzed and discussed in detail so far in the literature,
315 even though it is observed in many cases in RDE experiments, in both acidic [37,38] and alkaline
316 conditions [39–42]. It could be associated to the reduction of the O_2 adsorbed on the catalyst
317 surface, which occurs in concomitance with the reduction of the O_2 diffusing from the electrolyte
318 bulk. This phenomenon becomes evident because the LSV are non-steady-state experiments
319 (potential is varying linearly in time), and thus the appearance of peaks related to non-steady state
320 phenomena, as it is the case of the reduction of the O_2 adsorbed on the catalyst surface, may occur.
321 O_2 could have been enough time to adsorb on the catalyst surface (also considering the very high
322 specific surface area of this Fe-N-C catalyst, which is about 1500 $m^2\ g^{-1}$), and subsequently being
323 reduced during the voltammetric experiment, with the appearance of a peak similarly to what
324 happens in the CV plots in **Figure 1** and **Figure 2**. Additionally, some O_2 could adsorb on the
325 Nafion self-assemblies locally present on the catalyst surface [43,44], and could have enough time
326 to diffuse toward the ORR active sites and be reduced therein, since the LSV are performed at
327 moderately low scan rate (5 $mV\ s^{-1}$).

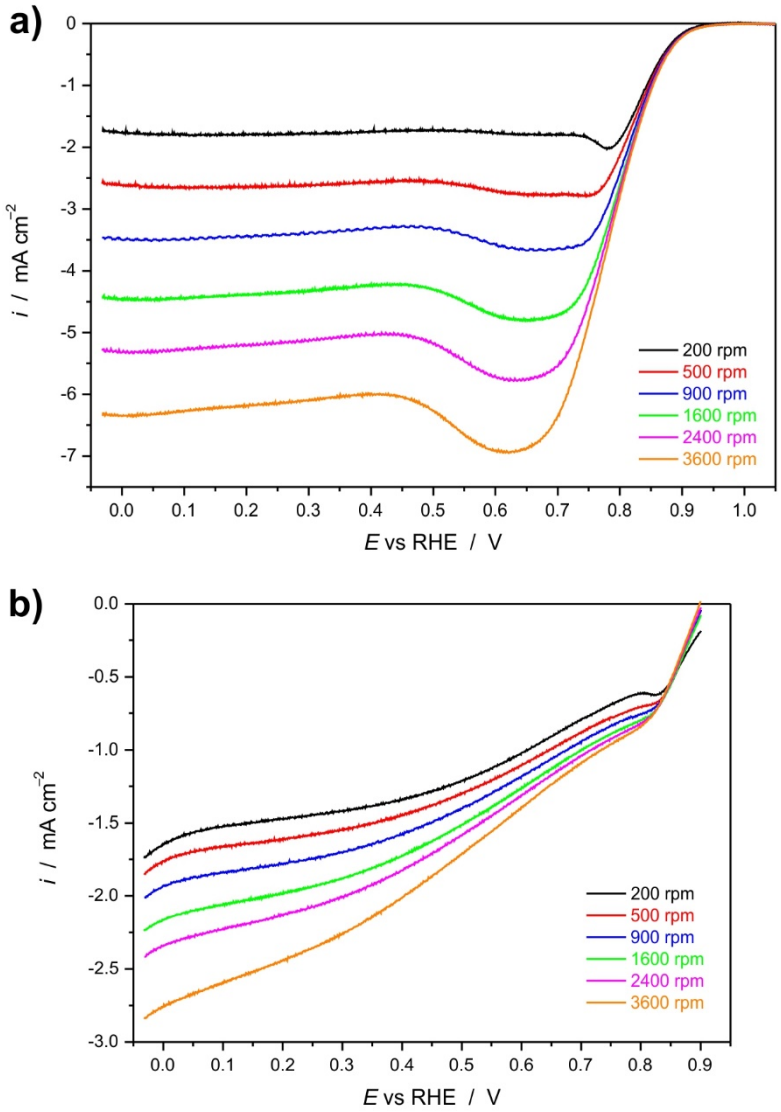

Fig. 3. (a) LSV recorded at 5 mV s^{-1} at different RDE rotation speeds in O_2-saturated 0.1 M KOH solution. The background current recorded under N_2-saturated 0.1 M KOH was subtracted to eliminate the contribution of the capacitive current. (b) LSV recorded at 5 mV s^{-1} at different RDE rotation speeds in N_2-saturated 0.1 M KOH solution containing H_2O_2 in 0.001 M concentration.

3.1.3. Ethanol tolerance test.

Since the Fe-N-C catalyst will be subsequently tested in an alkaline DEFC (see *Section 3.2*) the tolerance to ethanol of this catalyst is an important characteristic, even at the high potentials at which a DEFC cathode could work. In fact, ethanol could pass from the anodic to the cathodic compartment through the polymer electrolyte membrane. This is the well-known fuel crossover effect, which is one of the causes of the efficiency loss in a fuel cell system [45]. In alkaline electrolyte membrane fuel cells (AEMFC) the crossover effect is usually more limited than in acidic

PEMFC, due to the electroosmotic drag direction from cathode to anode [13,46], which partially hinders the permeation of alcohol and water through the membrane. The well-known activity of Pt-based catalysts toward the electro-oxidation of alcohols [47], in combination with the crossover effect, causes the presence of a mixed-potential at the fuel cell cathode, which in turns originates a decrease of the fuel cell E_{oc}.

In addition, the use of ethanol as a fuel is also an advantage, because the ethanol oxidation reaction (EOR) in alkaline conditions is only partial, and occurs mainly without the cleavage of the C–C bond, with the selective production of acetate [3,48]. As a consequence, the amount of CO (intermediate product of the oxidation of organic molecules containing a single C atom) that is formed is considerably lower in comparison with the use of methanol as a fuel. This low presence of CO is beneficial both for the anodic and the cathodic catalysts. In fact, CO tends to strongly chemisorb on the noble metal-based catalyst surface, causing a decrease in the activity [49]. Another consequence of the fact that EOR occurs without the cleavage of the C–C bond is the lower formation of CO_2, preventing damages to the alkaline electrolyte membrane. In fact, in alkaline conditions, the presence of CO_2 (and thus of CO_3^{2-} ions) causes the carbonation of the membrane, that is, the precipitation of K_2CO_3, which is also accelerated due to the presence of KOH in the solution fed to the anode [50,51].

All the aforementioned phenomena are the reasons why alkaline membrane DEFC usually show better power density compared to DMFC in both acidic and alkaline configuration, but also than DEFC in acidic configuration [52]. A further advantage of using ethanol as a fuel compared to methanol is that ethanol can be produced from renewable sources, *i.e.*, biomass fermentation [53,54]. Thus, the use of a noble-metal based catalyst at the cathode, besides the high costs, has the additional drawback of being subjected to deactivation caused by fuel crossover. This explains why it is highly desirable to operate alkaline DEFC with an NNM catalyst at the cathode. As reported in the literature, the Fe-N-C catalysts usually do not exhibit any activity towards the oxidation of alcohols, being highly selective towards ORR [12,19,21]. To demonstrate this also for our Fe-N-C

367 catalyst in alkaline conditions, we tested its ORR activity in 0.1 M KOH solution in presence of
368 different concentrations of ethanol, ranging from a minimum of 1 mM (almost the same
369 concentration of O_2 in the solution) to a maximum of 2 M (the concentration of ethanol in the
370 solution fed to the anode). The results shown in **Figure 4b** confirm that our Fe-N-C catalyst is
371 highly tolerant to the presence of ethanol. In fact, the ORR is occurring without any significant
372 modification in the polarization curve shape for all the ethanol concentrations. A slight decrease in
373 ORR activity is observed only for very high ethanol concentrations (1 M and 2 M), which are
374 almost impossible to be found at the DEFC cathode due to the crossover. This small activity
375 decrease, of ~ 40 mV negative shift in the half-wave potential from the test in the absence of
376 ethanol to the test with 2 M ethanol, can be attributable to a slight decrease of electrical
377 conductivity and O_2 solubility in the electrolyte solution with the increase of ethanol concentration.
378 A slight decrease in the limiting current density is also observed in the diffusion-limited part of the
379 polarization curve, that could also be caused by the decrease of O_2 content in the solution with
380 higher ethanol concentrations. This ethanol tolerance test indicates that the Fe-N-C catalyst is a
381 potentially good candidate to be used as a cathodic electrocatalyst in an alkaline DEFC.
382 The results obtained for the same test conducted on a Pt/C commercial catalyst (20 wt. % Pt on
383 Vulcan) are considerably different, as shown in **Figure 4c** (cathodic potential scan direction) and **4d**
384 (anodic potential scan direction). A remarkable decrease in ORR activity is observed for the Pt/C
385 catalyst already at ethanol concentrations as low as 0.005 M in the anodic scan direction, and 0.01
386 M in the cathodic scan direction. For higher concentrations of ethanol, big electro-oxidation peaks
387 are visible, confirming the much worse selectivity of Pt-based catalysts towards ORR in the
388 presence of ethanol compared to our Fe-N-C catalyst. The differences between the anodic and the
389 cathodic scan directions observed for Pt/C catalyst (see **Figures 4c** and **4d**) are due to the presence
390 of an oxide layer on the surface of Pt at high potentials, which is progressively removed during the
391 cathodic potential sweep, making the clean Pt surface totally available for the reaction of both O_2
392 and ethanol [55]. This oxide layer is not present during the anodic sweep scan, which starts at 0.0 V

vs. RHE, and thus from a Pt surface free from oxides that could hamper the reactions. This explains the different shape observed for the ethanol oxidation reaction peaks in the presence of oxygen in the two scan directions, and this is the cause of the well-known hysteresis effect observed in ORR experiments in RDE [56–58].

These differences are not observed for Fe-N-C catalyst, thus we only reported for this catalyst the cathodic scan direction (**Figure 4b**). The slightly higher values of the current density in the diffusion limiting plateau region (at high ORR overpotentials) measured for Fe-N-C catalyst compared to Pt/C can be attributed to the fact that the LSV in **Figure 4b**, **4c**, and **4d** were not corrected for the background capacitive current contribution, which is considerably higher for Fe-N-C than for Pt/C, as evidenced by **Figure 4a**.

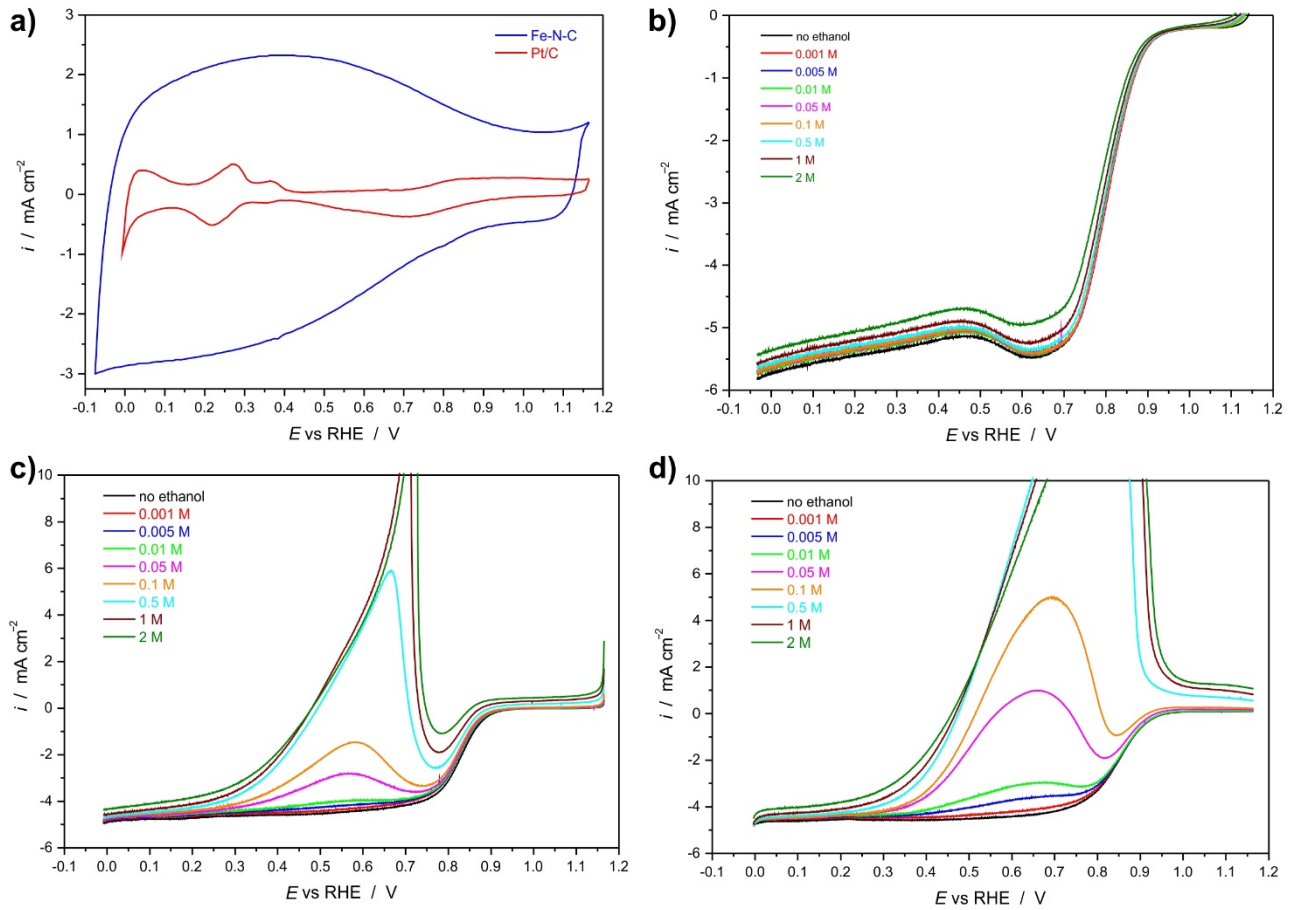

Fig. 4. (a) CV measured at 20 mV s^{-1} in N_2-saturated 0.1 M KOH solution for Fe-N-C catalyst and for the commercial Pt/C catalyst. (b) LSV measured in O_2-saturated 0.1 M KOH with different ethanol concentrations for Fe-N-C catalyst. (c) LSV measured in the cathodic scan direction in O_2-saturated 0.1 M KOH solution with different ethanol concentrations for the commercial Pt/C catalyst. (d) LSV measured in the anodic scan direction in O_2-saturated 0.1 M KOH solution with

409 different ethanol concentrations for the commercial Pt/C catalyst. In (b), (c), and (d) the LSV were
410 recorded at 5 mV s^{-1} and 1600 RDE rotation speed.
411

412 *3.1.4. Durability tests in RDE.*

413 The durability performance of the Fe-N-C catalyst in alkaline medium was assessed by two
414 different tests. First, the catalyst was cycled in a potential range of 1.0 – 0.6 V vs RHE, as also
415 reported in the literature, for example by X. Wang et al. [59]. This range was chosen considering
416 the potentials values at which the cathode of the fuel cell most likely works in practical
417 applications. The cycling was carried out in the O_2-saturated electrolyte. Full LSV polarization
418 curves were recorded at the beginning of the test, and then after 400, 4,000, and 10,000 cycles. The
419 results in **Figure 5a** show that the half-wave potential ($E_{1/2}$) only suffers a negative shift of 10 mV
420 after 400 cycles, 22 mV after 4000 cycles, and 33 mV after 10,000 cycles, evidencing a very good
421 resistance to potential cycling for Fe-N-C in the presence of O_2 under alkaline conditions.
422 To further investigate the durability of the catalyst, we carried out a chronoamperometry test during
423 48 hours at a fixed potential of 0.765 V vs RHE, which is almost corresponding to the half-wave
424 potential of the LSV polarization curve recorded at 1600 rpm (see **Figure 5a**). **Figure 5b** shows the
425 results of this test. At the beginning of the test the measured current density was 2.85 mA cm^{-2},
426 while after 48 hours of the test, this value decreased to 2.33 mA cm^{-2}, corresponding to a decrease
427 of about 18 %, thus confirming the considerably good stability performance of Fe-N-C catalyst in
428 alkaline conditions. As a comparison, we also performed the same chronoamperometry test for a
429 Pt/C catalyst. In this case, the initial current density was higher than for Fe-N-C catalyst (being
430 about 4.10 mA cm^{-2}), and it remained higher for all the duration of the test, decreasing to about
431 2.65 mA cm^{-2} after 48 hours. However, if we consider the relative percent current density decay
432 instead of the absolute value, Pt/C shows a worse performance, with a loss of about 36 % after 48
433 hours. The relative current density decay compared to the value measured at the beginning of the
434 test is show for both Fe-N-C and Pt/C catalysts in the inset of **Figure 5b**.

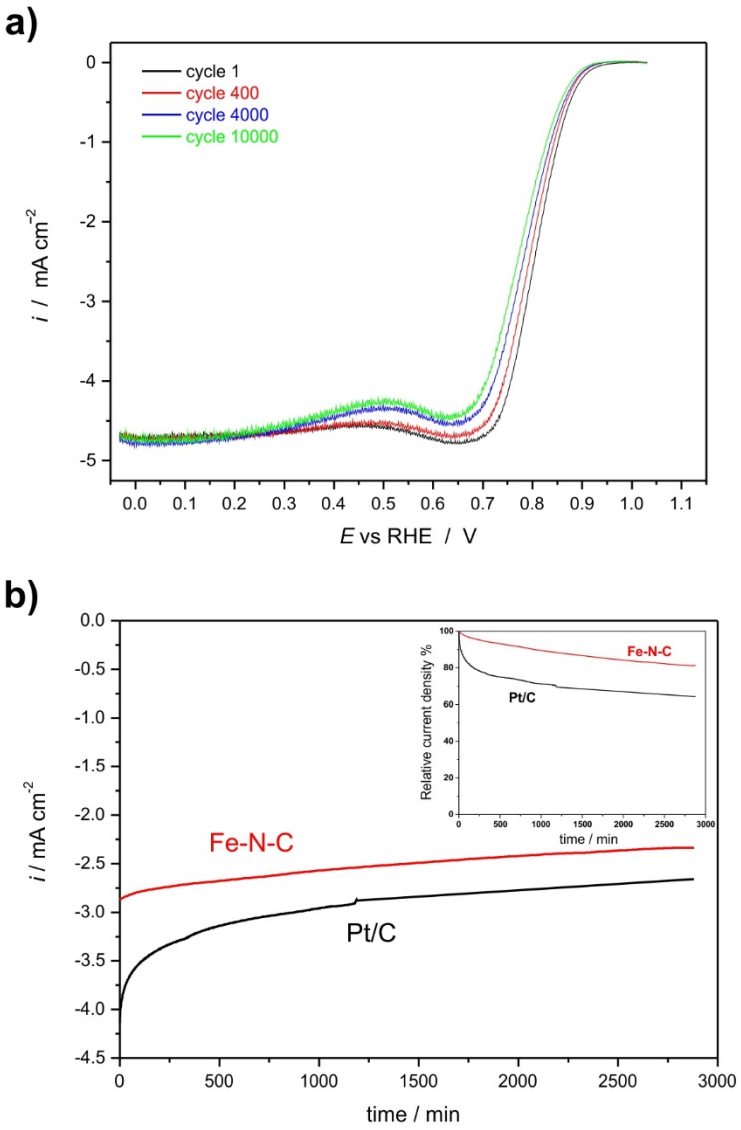

Fig. 5. (a) LSV recorded in O_2-saturated 0.1 M KOH at 1600 rpm and 5 mV s^{-1} after a different number of potential cycles between 1.0 and 0.6 V vs RHE for Fe-N-C catalyst. (b) Chronoamperometry test in RDE at 0.765 V vs. RHE for Fe-N-C and for a Pt/C catalyst in O_2-saturated 0.1 M KOH at 1600 rpm. The insert shows the relative % current decay.

We can attribute this good stability to the relatively high graphitic N content (which is close to 42 % atomic, see *Section 2.2*), which has been associated to a high catalyst stability in several literature works [60–62]. Another factor that could influence the catalyst stability is the graphitization degree of the carbonaceous matrix of the catalyst [63,64], which reaches a high value during the pyrolysis process, as demonstrated by the FTIR and Raman analyses reported in our previous work [22]. In a recent publication, a Fe-N-C catalyst synthesized using a silica template showed an enhanced

447 stability in alkaline media after 7500 potential cycles in RDE in 0.1 M KOH solution, similarly to
448 our catalyst [40].
449
450 *3.2. DEFC test.*
451 The Fe-N-C catalyst showed a very promising ORR performance in alkaline conditions in terms of
452 activity, selectivity, and durability in RDE. Thus, we tested it as a cathodic catalyst in an alkaline
453 DEFC. Moreover, the physicochemical properties of this catalyst (briefly reported in *Section 2.2*),
454 in particular in terms of overall surface area, as well as the promising results we obtained in acidic
455 DMFC tests in terms of short-term durability in comparison with the use of a commercial Pt/C
456 catalyst at the cathode [22], make this Fe-N-C catalyst of interest to be used as cathodic NNM
457 catalyst also for alkaline DAFC applications. To the best of our knowledge, there are only a few
458 studies in the literature showing the results of DEFC tests where a Me-N-C catalyst is used at the
459 cathode (see **Table 1**). Among them, even fewer studies show the stability and durability behavior
460 of the DEFC device.
461 As mentioned in the experimental section, to improve the DEFC performance, the anodic
462 compartment was fed with an aqueous solution containing both ethanol and KOH. As discussed in
463 the literature, the presence of OH^- ions in the anodic solution is helpful to enhance the performance
464 of a DEFC [48,65]. In facts, if ethanol is fed in a non-alkaline solution, the cell performance results
465 to be lower because the ionic conductivity of the ionomer is considerably lower than the
466 conductivity of a KOH solution, and providing an excess of OH^- ions in contact with the membrane
467 helps to enhance its conductivity. Moreover, being OH^- a reactant of the EOR in alkaline
468 conditions, an excess in the anodic compartment enhances the reaction kinetics as well [11,65].
469 **Figure 6a** shows the results of the alkaline DEFC tests using our Fe-N-C catalyst, and a
470 commercial Pt/C catalyst (40 wt. % Pt on Vulcan) at the cathode, for comparison purposes. For the
471 Fe-N-C, three different cathodic layers were prepared, with different Nafion® contents. Obviously,
472 the use of an H^+ conducing ionomer as Nafion® in the preparation of the catalytic layer of an

AEMFC does not favor the ionic conductivity. Nevertheless, the use of a PTFE-based ionomer in the preparation of electrodes for alkaline membrane fuel cells typically in amounts between 10 and 50 wt. % on the dry electrode is commonly reported in the literature [65–68]. As a matter of fact, the presence of a binder in the electrode is required to connect the catalyst particles together, preserving them from a progressive crumbling during the flushing of the reactants, which lead the cell performance to degrade quickly [65]. In addition, since the PTFE-like backbone of Nafion® is highly hydrophobic [43], the presence of this ionomer in the DEFC cathode catalyst layer can help the water removal during operation, reducing the detrimental cathode flooding effect.

As a confirmation of this, the performance of the alkaline DEFC we prepared with a low Nafion® content of 4 wt. % (on dry electrode basis) was the worst, showing a maximum power density of about 35 mW cm^{-2}. Increasing the Nafion® content to 35 %, the cell performances improved, reaching a maximum power density of 57 mW cm^{-2}, and becoming even slightly better at low current densities (until ~ 50 mA cm^{-2}) compared to the cell prepared using the commercial Pt/C catalyst at the cathode. The E_{oc} of this DEFC was also slightly higher than that of Pt/C (0.90 vs. 0.86 V). With a further increase of the Nafion® content until 50 wt. %, the performance of the cell at low current densities got worse. However, at a higher current density (approximately above 170 mA cm^{-2}) it slightly improved, getting a maximum power density of 62 mW cm^{-2}.

For all the different Nafion® contents, the polarization curve suffers a steep decrease almost immediately after the maximum power density. This behavior suggests that the DEFC performance was highly affected by mass transport limitation problems [46], which can hinder the diffusion of O_2 into the highly microporous cathodic catalyst layer [23,69]. In this regard, even if in alkaline fuel cells the H_2O as a product of the reaction is generated at the anode, the flooding of the cathode must not be excluded. As previously mentioned, this phenomenon can be reduced by the presence of the hydrophobic backbone in Nafion® ionomer. As demonstrated in the literature, the cathode flooding in AEMFC is likely to occur at intermediate current densities, contrarily to what happens in acidic electrolyte PEMFCs, where it occurs preferentially at high current densities [26].

499 The results obtained with different Nafion® contents in the cathode suggest that the presence of an
500 ionomer acting as a binder is useful to obtain better performances in DEFC, even if the ionomer is
501 not an OH^- conductor. However, the Nafion® content must be optimized to determine the quantity
502 that allows obtaining the better performance. In the case of our Fe-N-C catalyst, the optimal
503 Nafion® loading ranges between 35 and 50 wt. %. Nafion® ionomer can modify the surface
504 properties of the catalyst layer by modifying mechanical proprieties, and consequently the chemical
505 affinity of reactants/products [70].
506 For the DEFC prepared using the Pt/C catalyst at the cathode, these mass transport problems are
507 less evident. They start to occur at higher current densities, enabling to obtain a considerably higher
508 maximum power density (~ 88 mW cm^{-2}), although the E_{oc} was almost the same, or even worse
509 compared to the tests with Fe-N-C catalyst.
510 From the polarization curves in **Figure 6a**, it is possible to have an approximated idea of the cell
511 ohmic resistance from the linear zone of the polarization curve at intermediate current densities,
512 where the limiting factor are mainly the ohmic losses [71]. A higher slope of this linear zone of the
513 polarization curve is an indication of a higher ohmic cell resistance.
514 As reported in a work recently published by our group [12], to assess the durability performance of
515 this type of alkaline DEFC is not trivial. In fact, this system has shown intrinsic stability issues,
516 which can be attributable to instability of the membrane conductivity [48], to the MEA fabrication
517 procedure (absence of hot-pressing, poor compatibility between the membrane and the ionomer
518 used for the catalyst ink preparation), to mass transport issues (flooding of catalyst layer), and Ru
519 electro-dissolution/crossover [72]. **Figure 6b** shows the polarization and power density curves of
520 the best performing MEA (the one prepared using 50 wt. % Nafion®) at the beginning of the test
521 (the same of **Figure 6a**), and after 20 consecutive recording of polarization curves. The DEFC
522 shows a remarkable decrease of the maximum power density, from 62 to 24 mW cm^{-2}, suggesting a
523 very poor stability performance.

524 Interestingly, after a purge/drying reactivation procedure developed in our laboratory [12], which
525 consists in flowing dry N_2 at 90 °C for 30 minutes in both anodic and cathodic compartments of the
526 cell, it is evident that the initial performance can be partially recovered, obtaining a maximum
527 power density of 41 mW cm^{-2}. These results are in agreement with the results described in our
528 recent work for other Fe-N/C catalysts [12]. However, all the catalysts reported in our previous
529 work show a better performance in terms of reactivation compared to the Fe-N-C catalysts
530 presented in this work. This could be attributed to the much higher specific surface area and
531 microporosity of this catalysts compared to the previous ones, causing more mass transport issues.
532 In particular, the small micropores are more prone to flooding, which can also be partially
533 irreversible [69,73].
534 These results are a confirmation that the huge DEFC performance losses in the short-term cannot be
535 attributed exclusively to the irreversible deactivation of the Fe-N-C catalyst.
536 Regarding the possible carbonation of the alkaline electrolyte membrane, which can occur due to
537 the formation of CO_2 as EOR reaction product at the anode (as previously discussed in *Section*
538 *3.1.3*), several literature works demonstrate that in both alkaline and acidic media, with all the most
539 commonly used catalysts for EOR (including Pt-Ru, which was used as anodic catalyst in our
540 DEFC test), the selectivity of formation of CO_2 at potentials values normally present at the anode of
541 a DEFC during operation is low [74–78]. This would most likely avoid the occurrence of a massive
542 carbonation of the alkaline membrane, at least in the short-term period, letting us to deduce that the
543 membrane carbonation has not to be ascribed as one of the causes of the fast DEFC performance
544 decay we observed.
545 By concluding, the performance of our Fe-N-C as a cathodic catalyst for alkaline DEFC is good in
546 terms of power density and open circuit potential, especially at low-intermediate current densities,
547 confirming the good results obtained for ORR activity and ethanol tolerance in the RDE tests.
548 However, the sharp DEFC performance decrease at high current density compared to the
549 commercial Pt/C catalyst, as well as the results of the short-term durability and reactivation test

(also in comparison to other catalysts of our group [12]), evidenced that this Fe-N-C catalyst still shows mass transport problems, and its features may have to be optimized accordingly, for example reducing the overall and microporous specific surface area.

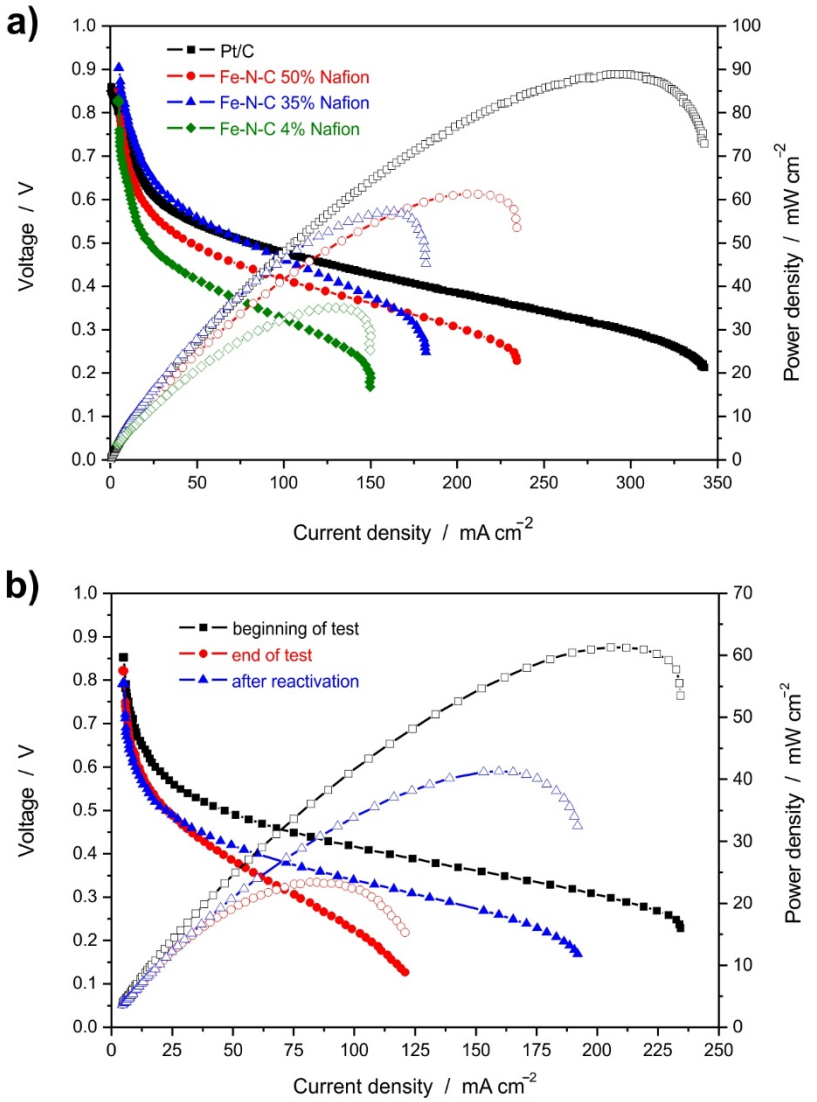

Fig. 6. (a) Polarization curves (filled symbols) and power density curves (open symbols) for alkaline DEFC prepared using Fe-N-C as a cathodic catalyst with different Nafion® contents. The curves for a DEFC prepared using a commercial Pt/C catalyst are also shown for comparison. (b) Short-term durability test in alkaline DEFC for Fe-N-C 50 wt. % Nafion®. Polarization curves (filled symbols) and power density curves (open symbols) recorded at the beginning of the test (black), at the end of the test (red), and after the purge-drying reactivation procedure (blue).

Table 1 resumes the results available so far in the literature about the performances of alkaline DEFC prepared using NNM cathodic catalysts. Our results can be considered comparable to the

563 best State-of-the-Art, taking into account the different testing conditions (i.e. anodic catalyst,

564 catalyst loading, membrane, ionomer, temperature, etc.) reported in **Table 1**.

565

566 **Table 1.** State-of-the-Art performances in alkaline membrane DEFC using NNM catalysts at the
567 cathode.

Ref.	Cathode Catalyst	Anode Catalyst	Membrane	DEFC Test conditions	Max Power Density (mW cm^{-2})	Max Power Density (mW $mg^{-1}_{NobleMetal}$)
[68]	Commercial Acta S.p.A Hypermec^{tm} K14 3.5 mg cm^{-2}	Commercial Acta S.p.A Hypermec^{tm} 3020 Series 15 mg cm^{-2}	5 cm^2 Tokuyama A-006 (OH form), sandwiched without hot pressing	10 wt. % EtOH – 10 wt. % KOH O_2 0% RH 60 °C	90	
[66]	NiMnOx/C 3 mg cm^{-2}	PtRu/C 0.5 mg cm^{-2}	4.62 cm^2 PBI (pre-treated with 6 M KOH)	2 M EtOH – 3 M KOH O_2 90 °C	55	~110
[79]	Commercial Catalyst Fe-Co Hypermec^{tm}	Pd/MWCNT 1 mg cm^{-2}	Tokuyama A-006	80 °C	73	~73
[80]	40% MnO_2/C 1 mg cm^{-2}	40%Pd/C 2 mg cm^{-2}	4 cm^2 Nafion® 112 pre treated with 6M KOH	1 mL min^{-1} 2M EtOH – 2M KOH Air atmospheric pressure (Air breath) 60 °C	11.5	~5.75
[81]	CoTMPhP/C heat treat at 850°C for 2 h in Ar, 9.2 mg cm^{-2}, after depositing on GDL the electrode was tempered at 360 °C for 20 min in Ar	RuV/C (3:2 at%) 20 or 40 wt. % on C ink prepared using Fumion® ionomer 4.5 mg cm^{-2}	5 cm^2 PBI doped in 3M KOH + 2M EtOH for 48h	5 mL min^{-1} 3M KOH + 2M EtOH 0.2 L min^{-1} Air 80 °C	100	~44
[82]	Commercial Acta S.p.A Hypermec^{tm} 1 mg cm^{-2}	Commercial Acta S.p.A Hypermec^{tm} 2 mg cm^{-2}	4 cm^2 Tokuyama A201 without hot pressing	1M EtOH – 3 M KOH 3 mL min^{-1} 400 sscm Pure O_2 40 °C	60	~30
[54]	Fe-Co/C, heat treated at 600 °C. The cathode was heated at 340 °C for 20 min in Ar	Pd/TNTA (Titanium Nanotube Array) 6 mg Pd cm^{-2}	25 cm^2 Tokuyama A201	2M KOH and EtOH 10 wt% 80 °C	335	~55
[83]	Fe-Co/C, heat treated at 600 °C. The cathode was heated at 340 °C for 20 min in Ar	Pd-CeO_2/C 1 mg cm^{-2}	5 cm^2 Tokuyama A-006 commercial mechanical pressing of anode, cathode, and membrane	4 mL min^{-1} 10 wt % EtOH – 2M KOH 200 mL min^{-1} O_2 80 °C	140	~140

[12]	Fe-N/MPC, Fe-phenanthroline on mesoporous carbon, heat treated at 800 °C 2.5 mg cm^{-2}	Pt-Ru/C 45 wt. % 1.33 mg cm^{-2}	2.89 cm^2 PBI (Danish Power Systems) doped with 6 M KOH not hot pressing	1 mL min^{-1} 2M EtOH – 2M KOH 200 NmL min^{-1} pure O_2 (3 bar brackpressure) 90 °C	75	~56
This work	Fe-N-C	Pt-Ru/C 45 wt. % 1.33 mg cm^{-2}	2.89 cm^2 PBI (Danish Power Systems) doped with 6 M KOH not hot pressing	1 mL min^{-1} 2M EtOH – 2M KOH 200 NmL min^{-1} pure O_2 (3 bar brackpressure) 90 °C	62	~47

4. Conclusions

The electrochemical performance of a Fe-N-C catalyst synthesized using Fe(II)-phthalocyanine via hard templating method was investigated in alkaline medium. The cathodic transfer coefficient calculated for the reduction of the oxygen adsorbed on the catalyst surface by CV coincides with the one measured by the Tafel plot recorded by RDE test at low overpotentials. The cathodic transfer coefficient changes with the potential, indicating a change in ORR mechanism by varying the potential. The results of the ORR and HPRR tests (in combination with the results and the RRDE test reported in our previous work [23]) indicate that the ORR in an alkaline medium mainly occurs following the direct 4 e^- reduction to OH^-. The Fe-N-C catalyst was also found to be tolerant to the presence of ethanol, and it had a very good stability and durability in RDE, which make it a promising candidate for application as a cathodic catalyst in alkaline DEFC. The alkaline DEFC test demonstrated this good potentiality, being the maximum power density reached in DEFC (after the optimization of the ionomer content on the electrode) comparable to the best state-of-the-art results reported in the literature for DEFC prepared using NNM catalysts. However, the DEFC performance shows a steep decay at high current densities, which are mainly ascribed to mass transport problems (flooding and/or O_2 diffusion) caused by the high microporosity of the catalyst. The poor intrinsic stability of this alkaline DEFC system is also evidenced.

Acknowledgments

This work was supported by the Madrid Regional Research Council (CAM) [RESTOENE-2 grant n. S2013/MAE2882], the Spanish Economy and Competitiveness Ministry [ENE2016 grant n. 77055-C3-1-R], and the Italian Ministry of Education, University and Research [PRIN NAMEDPEM grant n. 2010CYTWAW].

References

[1] S. Endoo, K. Pruksathorn, P. Piumsomboon, Identification of the key variables in membrane electrode preparation for PEM fuel cells by a factorial design, Renew. Energy. 35 (2010) 807–813. doi:10.1016/j.renene.2009.10.013.

[2] S.-Y. Huang, P. Ganesan, B.N. Popov, Titania supported platinum catalyst with high electrocatalytic activity and stability for polymer electrolyte membrane fuel cell, Appl. Catal. B Environ. 102 (2011) 71–77. doi:10.1016/j.apcatb.2010.11.026.

[3] L. Wang, A. Lavacchi, M. Bellini, F. D'Acapito, F. Di Benedetto, M. Innocenti, H.A. Miller, G. Montegrossi, C. Zafferoni, F. Vizza, Deactivation of Palladium Electrocatalysts for Alcohols Oxidation in Basic Electrolytes, Electrochim. Acta. 177 (2015) 100–106. doi:10.1016/j.electacta.2015.02.026.

[4] X. Li, B.N. Popov, T. Kawahara, H. Yanagi, Non-precious metal catalysts synthesized from precursors of carbon, nitrogen, and transition metal for oxygen reduction in alkaline fuel cells, J. Power Sources. 196 (2011) 1717–1722. doi:10.1016/j.jpowsour.2010.10.018.

[5] M.M. Mench, H.M. Chance, C.Y. Wang, Direct Dimethyl Ether Polymer Electrolyte Fuel Cells for Portable Applications, J. Electrochem. Soc. 151 (2004) A144. doi:10.1149/1.1631819.

[6] M. Simões, S. Baranton, C. Coutanceau, Electro-oxidation of glycerol at Pd based nano-catalysts for an application in alkaline fuel cells for chemicals and energy cogeneration, Appl. Catal. B Environ. 93 (2010) 354–362. doi:10.1016/j.apcatb.2009.10.008.

[7] N. Benipal, J. Qi, J.C. Gentile, W. Li, Direct glycerol fuel cell with polytetrafluoroethylene

(PTFE) thin film separator, Renew. Energy. 105 (2017) 647–655. doi:10.1016/j.renene.2016.12.028.

[8] S. Specchia, C. Francia, P. Spinelli, Polymer Electrolyte Membrane Fuel Cells, in: J. Zhang, L. Zhang, H. Liu, A. Sun, R.-S. Liu (Eds.), Electrochem. Technol. Energy Storage Convers., WILEY-VCH Verlag, Weinheim, 2011: pp. 601–670. doi:10.1002/9783527639496.

[9] S.K. Nataraj, C.H. Wang, H.C. Huang, H.Y. Du, S.F. Wang, Y.C. Chen, L.C. Chen, K.H. Chen, Highly proton-selective biopolymer layer-coated ion-exchange membrane for direct methanol fuel cells, ChemSusChem. 5 (2012) 392–395. doi:10.1002/cssc.201100366.

[10] D. Sebastián, V. Baglio, S. Sun, A.C. Tavares, A.S. Aricò, Graphene-supported substoichiometric sodium tantalate as a methanol-tolerant, non-noble-metal catalyst for the electroreduction of oxygen, ChemCatChem. 7 (2015) 911–915. doi:10.1002/cctc.201403026.

[11] L. Jiang, A. Hsu, D. Chu, R. Chen, Ethanol electro-oxidation on Pt/C and PtSn/C catalysts in alkaline and acid solutions, Int. J. Hydrogen Energy. 35 (2010) 365–372. doi:10.1016/j.ijhydene.2009.10.058.

[12] L. Osmieri, R. Escudero-Cid, M. Armandi, A.H.A. Monteverde Videla, J.L.G. Fierro, P. Ocón, S. Specchia, Fe-N/C catalysts for oxygen reduction reaction supported on different carbonaceous materials. Performance in acidic and alkaline direct alcohol fuel cells., Appl. Catal. B Environ. 205 (2017) 637–653. doi:10.1016/j.apcatb.2017.01.003.

[13] V.V. Shevchenko, M. a. Gumennaya, Synthesis and properties of anion-exchange membranes for fuel cells, Theor. Exp. Chem. 46 (2010) 139–152. doi:10.1007/s11237-010-9131-4.

[14] L. An, T.S. Zhao, Y.S. Li, Carbon-neutral sustainable energy technology: Direct ethanol fuel cells, Renew. Sustain. Energy Rev. 50 (2015) 1462–1468. doi:10.1016/j.rser.2015.05.074.

[15] R. Othman, A.L. Dicks, Z. Zhu, Non precious metal catalysts for the PEM fuel cell cathode, Int. J. Hydrogen Energy. 37 (2012) 357–372. doi:10.1016/j.ijhydene.2011.08.095.

[16] J.K. Dombrovskis, A.E.C. Palmqvist, Recent Progress in Synthesis, Characterization and

640 Evaluation of Non-Precious Metal Catalysts for the Oxygen Reduction Reaction, Fuel Cells.
641 16 (2016) 4–22. doi:10.1002/fuce.201500123.
642 [17] L. Osmieri, A.H.A. Monteverde Videla, S. Specchia, Optimization of a Fe-N-C
643 electrocatalyst supported on ordered mesoporous carbon functionalized with polypyrrole for
644 oxygen reduction reaction Optimization of a Fe-N-C electrocatalyst supported on ordered
645 mesoporous carbon functionalized with polypyrrole f, Int. J. Hydrogen Energy. 41 (2016)
646 19610–19628. doi:10.1016/j.ijhydene.2016.05.270.
647 [18] D. Sebastián, A. Serov, I. Matanovic, K. Artyushkova, P. Atanassov, A.S. Aricò, V. Baglio,
648 Insights on the extraordinary tolerance to alcohols of Fe-N-C cathode catalysts in highly
649 performing direct alcohol fuel cells, Nano Energy. 34 (2017) 195–204.
650 doi:10.1016/j.nanoen.2017.02.039.
651 [19] D. Sebastián, V. Baglio, A.S. Aricò, A. Serov, P. Atanassov, Performance analysis of a non-
652 platinum group metal catalyst based on iron-aminoantipyrine for direct methanol fuel cells,
653 Appl. Catal. B Environ. 182 (2015) 297–305. doi:10.1016/j.apcatb.2015.09.043.
654 [20] A. Serov, K. Artyushkova, N.I. Andersen, S. Stariha, P. Atanassov, Original
655 Mechanochemical Synthesis of Non-Platinum Group Metals Oxygen Reduction Reaction
656 Catalysts Assisted by Sacrificial Support Method, Electrochim. Acta. 179 (2015) 154–160.
657 doi:10.1016/j.electacta.2015.02.108.
658 [21] D. Sebastián, A. Serov, K. Artyushkova, P. Atanassov, A.S. Aricò, V. Baglio, Performance,
659 methanol tolerance and stability of Fe-aminobenzimidazole derived catalyst for direct
660 methanol fuel cells, J. Power Sources. 319 (2016) 235–246.
661 doi:10.1016/j.jpowsour.2016.04.067.
662 [22] L. Osmieri, R. Escudero-cid, A.H.A. Monteverde Videla, P. Ocón, S. Specchia, Performance
663 of a Fe-N-C catalyst for the oxygen reduction reaction in direct methanol fuel cell : Cathode
664 formulation optimization and short-term durability, Appl. Catal. B Environ. 201 (2017) 253–
665 265. doi:10.1016/j.apcatb.2016.08.043.

[23] L. Osmieri, A.H.A. Monteverde Videla, M. Armandi, S. Specchia, Influence of different transition metals on the properties of Me-N-C (Me = Fe, Co, Cu, Zn) catalysts synthesized using SBA-15 as tubular nano-silica reactor for oxygen reduction reaction, Int. J. Hydrogen Energy. 41 (2016) 22570–22588. doi:10.1016/j.ijhydene.2016.05.223.

[24] R. Escudero-cid, Estudio de Durabilidad de Pilas de Combustible de Metanol Directo, Universidad Autónoma de Madrid, 2015.

[25] R. Escudero-Cid, M. Montiel, L. Sotomayor, B. Loureiro, E. Fatás, P. Ocón, Evaluation of polyaniline-Nafion® composite membranes for direct methanol fuel cells durability tests, Int. J. Hydrogen Energy. 40 (2015) 8182–8192. doi:10.1016/j.ijhydene.2015.04.130.

[26] Y.S. Li, T.S. Zhao, R. Chen, Cathode flooding behaviour in alkaline direct ethanol fuel cells, J. Power Sources. 196 (2011) 133–139. doi:10.1016/j.jpowsour.2010.06.111.

[27] L. Osmieri, A.H.A. Monteverde Videla, S. Specchia, Activity of Co–N multi walled carbon nanotubes electrocatalysts for oxygen reduction reaction in acid conditions, J. Power Sources. 278 (2015) 296–307. doi:10.1016/j.jpowsour.2014.12.080.

[28] L. Osmieri, A.H.A. Monteverde Videla, S. Specchia, The use of different types of reduced graphene oxide in the preparation of Fe-N-C electrocatalysts: capacitive behavior and oxygen reduction reaction activity in alkaline medium, J. Solid State Electrochem. 20 (2016) 3507–3523. doi:10.1007/s10008-016-3332-2.

[29] R. Greef, R. Peat, L.M. Peter, D. Pletcher, J. Robinson, Instrumental Methods in Electrochemistry, Ellis Horwood Limited, Chichester, West Sussex, England, 1985.

[30] E. Laviron, General Expression of the Linear Potential Sweep Voltammogram in the case of Diffusionless Electrochemical Systems, J. Electroanal. Chem. 101 (1979) 19–28.

[31] J. Chlistunoff, RRDE and Voltammetric Study of ORR on Pyrolyzed Fe / Polyaniline Catalyst . On the Origins of Variable Tafel Slopes, J. Phys. Chem. C. 115 (2011) 6496–6507.

[32] R. Guidelli, R.G. Compton, J.M. Feliu, E. Gileadi, J. Lipkowski, W. Schmickler, S. Trasatti, Defining the transfer coefficient in electrochemistry: An assessment (IUPAC Technical

692 Report), Pure Appl. Chem. 86 (2014) 245–258. doi:10.1515/pac-2014-5026.
693 [33] L. Xu, G. Pan, X. Shi, C. Zou, Y. Zhou, G. Luo, G. Chen, A non-noble material cathode
694 catalyst dual-doped with sulfur and nitrogen as efficient electrocatalysts for oxygen reduction
695 reaction, Electrochim. Acta. 177 (2015) 57–64. doi:10.1016/j.electacta.2015.01.107.
696 [34] T. Lopes, A. Kucernak, D. Malko, E.A. Ticianelli, Mechanistic Insights into the Oxygen
697 Reduction Reaction on Metal–N–C Electrocatalysts under Fuel Cell Conditions,
698 ChemElectroChem. 3 (2016) 1580–1590. doi:10.1002/celc.201600354.
699 [35] J. Masa, C. Batchelor-McAuley, W. Schuhmann, R.G. Compton, Koutecky-Levich analysis
700 applied to nanoparticle modified rotating disk electrodes: Electrocatalysis or
701 misinterpretation, Nano Res. 7 (2013) 71–78. doi:10.1007/s12274-013-0372-0.
702 [36] R. Zhou, Y. Zheng, M. Jaroniec, S.-Z. Qiao, Determination of the Electron Transfer Number
703 for the Oxygen Reduction Reaction: From Theory to Experiment, ACS Catal. 6 (2016) 4720–
704 4728. doi:10.1021/acscatal.6b01581.
705 [37] F. Jaouen, V. Goellner, M. Lefèvre, J. Herranz, E. Proietti, J.P. Dodelet, Oxygen reduction
706 activities compared in rotating-disk electrode and proton exchange membrane fuel cells for
707 highly active FeNC catalysts, Electrochim. Acta. 87 (2013) 619–628.
708 doi:10.1016/j.electacta.2012.09.057.
709 [38] F. Jaouen, J. Herranz, M. Lefèvre, J.-P. Dodelet, U.I. Kramm, I. Herrmann, P. Bogdanoff, J.
710 Maruyama, T. Nagaoka, A. Garsuch, J.R. Dahn, T. Olson, S. Pylypenko, P. Atanassov, E. a
711 Ustinov, Cross-laboratory experimental study of non-noble-metal electrocatalysts for the
712 oxygen reduction reaction., ACS Appl. Mater. Interfaces. 1 (2009) 1623–39.
713 doi:10.1021/am900219g.
714 [39] D. Geng, H. Liu, Y. Chen, R. Li, X. Sun, S. Ye, S. Knights, Non-noble metal oxygen
715 reduction electrocatalysts based on carbon nanotubes with controlled nitrogen contents, J.
716 Power Sources. 196 (2011) 1795–1801. doi:10.1016/j.jpowsour.2010.09.084.
717 [40] R. Gokhale, Y. Chen, A. Serov, K. Artyushkova, P. Atanassov, Novel dual templating

718 approach for preparation of highly active Fe-N-C electrocatalyst for oxygen reduction,
719 Electrochim. Acta. 224 (2017) 49–55. doi:10.1016/j.electacta.2016.12.052.
720 [41] K. Niu, B. Yang, J. Cui, J. Jin, X. Fu, Q. Zhao, J. Zhang, Graphene-based non-noble-metal
721 Co/N/C catalyst for oxygen reduction reaction in alkaline solution, J. Power Sources. 243
722 (2013) 65–71. doi:10.1016/j.jpowsour.2013.06.007.
723 [42] F. Pan, Z. Cao, Q. Zhao, H. Liang, J. Zhang, Nitrogen-doped porous carbon nanosheets made
724 from biomass as highly active electrocatalyst for oxygen reduction reaction, J. Power
725 Sources. 272 (2014) 8–15. doi:10.1016/j.jpowsour.2014.07.180.
726 [43] J. Chlistunoff, J.-M. Sansiñena, On the use of Nafion® in electrochemical studies of carbon
727 supported oxygen reduction catalysts in aqueous media, J. Electroanal. Chem. 780 (2016)
728 134–146. doi:10.1016/j.jelechem.2016.09.014.
729 [44] J. Chlistunoff, J.-M. Sansiñena, Nafion Induced Surface Confinement of Oxygen in Carbon-
730 Supported Oxygen Reduction Catalysts, J. Phys. Chem. C. 120 (2016) 28038–28048.
731 doi:10.1021/acs.jpcc.6b09523.
732 [45] R. Escudero Cid, J.L. Gõmez De La Fuente, S. Rojas, J.L. García Fierro, P. Ocón,
733 Polypyrrole-modified-carbon-supported Ru-Pt nanoparticles as highly methanol-tolerant
734 electrocatalysts for the oxygen-reduction reaction, ChemCatChem. 5 (2013) 3680–3689.
735 doi:10.1002/cctc.201300448.
736 [46] H. Li, Y. Tang, Z. Wang, Z. Shi, S. Wu, D. Song, J. Zhang, K. Fatih, J. Zhang, H. Wang, Z.
737 Liu, R. Abouatallah, A. Mazza, A review of water flooding issues in the proton exchange
738 membrane fuel cell, J. Power Sources. 178 (2008) 103–117.
739 doi:10.1016/j.jpowsour.2007.12.068.
740 [47] R. Escudero-Cid, J.C. Pérez-Flores, E. Fatás, P. Ocón, Degradation of DMFC using a New
741 Long-Term Stability Cycle, Int. J. Green Energy. 12 (2015) 641–653.
742 doi:10.1080/15435075.2013.867269.
743 [48] H. Hou, S. Wang, Q. Jiang, W. Jin, L. Jiang, G. Sun, Durability study of KOH doped

744 polybenzimidazole membrane for air-breathing alkaline direct ethanol fuel cell, J. Power
745 Sources. 196 (2011) 3244–3248. doi:10.1016/j.jpowsour.2010.11.104.
746 [49] R. Escudero-Cid, P. Hernández-Fernández, J.C. Pérez-Flores, S. Rojas, S. Garcia-Rodríguez,
747 E. Fatás, P. Ocón, Analysis of performance losses of direct methanol fuel cell with methanol
748 tolerant PtCoRu/C cathode electrode, Int. J. Hydrogen Energy. 37 (2012) 7119–7130.
749 doi:10.1016/j.ijhydene.2011.12.158.
750 [50] E. Antolini, E.R. Gonzalez, Alkaline direct alcohol fuel cells, J. Power Sources. 195 (2010)
751 3431–3450. doi:10.1016/j.jpowsour.2009.11.145.
752 [51] C.-C. Yang, Alkaline direct methanol fuel cell based on a novel anion-exchange composite
753 polymer membrane, J. Appl. Electrochem. 42 (2012) 305–317. doi:10.1007/s10800-012-
754 0395-3.
755 [52] A.L. Mohana Reddy, N. Rajalakshmi, S. Ramaprabhu, Cobalt-polypyrrole-multiwalled
756 carbon nanotube catalysts for hydrogen and alcohol fuel cells, Carbon N. Y. 46 (2008) 2–11.
757 doi:10.1016/j.carbon.2007.10.021.
758 [53] Y. Wang, S. Zou, W.-B. Cai, Recent Advances on Electro-Oxidation of Ethanol on Pt- and
759 Pd-Based Catalysts: From Reaction Mechanisms to Catalytic Materials, Catalysts. 5 (2015)
760 1507–1534. doi:10.3390/catal5031507.
761 [54] Y. Chen, M. Bellini, M. Bevilacqua, P. Fornasiero, A. Lavacchi, H.A. Miller, L. Wang, F.
762 Vizza, Direct Alcohol Fuel Cells: Toward the Power Densities of Hydrogen-Fed Proton
763 Exchange Membrane Fuel Cells, ChemSusChem. 8 (2015) 524–533.
764 doi:10.1002/cssc.201402999.
765 [55] I.A. Pasti, N.M. Gavrilov, S.V. Mentus, Potentiodynamic investigation of oxygen reduction
766 reaction on polycrystalline platinum surface in acidic solutions: The effect of the polarization
767 rate on the kinetic parameters, Int. J. Electrochem. Sci. 7 (2012) 11076–11090.
768 [56] A.M. Gómez-Marín, R. Rizo, J.M. Feliu, Some reflections on the understanding of the
769 oxygen reduction reaction at Pt(111), Beilstein J. Nanotechnol. 4 (2013) 956–967.

doi:10.3762/bjnano.4.108.

[57] N.M. Markovic, T.J. Schmidt, B.N. Grgur, H.A. Gasteiger, R.J. Behm, P.N. Ross, Effect of Temperature on Surface Processes at the Pt (111) - Liquid Interface : Hydrogen Adsorption , Oxide Formation , and CO Oxidation, J. Phys. Chem. B. 103 (1999) 8568–8577. doi:10.1021/jp991826u.

[58] S. Mukerjee, S. Srinivasan, Enhanced electrocatalysis of oxygen reduction on platinum alloys in proton exchange membrane fuel cells, J. Electroanal. Chem. 357 (1993) 201–224. doi:10.1016/0022-0728(93)80380-Z.

[59] X. Wang, H. Zhang, H. Lin, S. Gupta, C. Wang, Z. Tao, H. Fu, T. Wang, J. Zheng, G. Wu, X. Li, Directly Converting Fe−doped Metal-Organic Frameworks into Highly Active and Stable Fe−N-C Catalysts for Oxygen Reduction in Acid, Nano Energy. 510 (2016) 426–436. doi:10.1016/j.nanoen.2016.04.042.

[60] H.R. Byon, J. Suntivich, Y. Shao-Horn, Graphene-Based Non-Noble-Metal Catalysts for Oxygen Reduction Reaction in Acid, Chem. Mater. 23 (2011) 3421–3428. doi:10.1021/cm2000649.

[61] G. Liu, X. Li, P. Ganesan, B.N. Popov, Studies of oxygen reduction reaction active sites and stability of nitrogen-modified carbon composite catalysts for PEM fuel cells, Electrochim. Acta. 55 (2010) 2853–2858. doi:10.1016/j.electacta.2009.12.055.

[62] G. Liu, X. Li, P. Ganesan, B.N. Popov, Development of non-precious metal oxygen-reduction catalysts for PEM fuel cells based on N-doped ordered porous carbon, Appl. Catal. B Environ. 93 (2009) 156–165. doi:10.1016/j.apcatb.2009.09.025.

[63] F. Charreteur, F. Jaouen, S. Ruggeri, J.-P. Dodelet, Fe/N/C non-precious catalysts for PEM fuel cells: Influence of the structural parameters of pristine commercial carbon blacks on their activity for oxygen reduction, Electrochim. Acta. 53 (2008) 2925–2938. doi:10.1016/j.electacta.2007.11.002.

[64] H.-S. Oh, J.-G. Oh, B. Roh, I. Hwang, H. Kim, Development of highly active and stable non-

precious oxygen reduction catalysts for PEM fuel cells using polypyrrole and a chelating agent, Electrochem. Commun. 13 (2011) 879–881. doi:10.1016/j.elecom.2011.05.027.

[65] Y.S. Li, T.S. Zhao, Z.X. Liang, Effect of polymer binders in anode catalyst layer on performance of alkaline direct ethanol fuel cells, J. Power Sources. 187 (2009) 387–392. doi:10.1016/j.jpowsour.2008.10.132.

[66] A.C. Garcia, J.J. Linares, M. Chatenet, E. a. Ticianelli, NiMnOx/C: A Non-noble Ethanol-Tolerant Catalyst for Oxygen Reduction in Alkaline Exchange Membrane DEFC, Electrocatalysis. 5 (2013) 41–49. doi:10.1007/s12678-013-0162-1.

[67] A.N. Geraldes, D.F. da Silva, L.G.D.A. e Silva, E.V. Spinacé, A.O. Neto, M.C. dos Santos, Binary and ternary palladium based electrocatalysts for alkaline direct glycerol fuel cell, J. Power Sources. 293 (2015) 823–830. doi:10.1016/j.jpowsour.2015.06.010.

[68] M. Zhiani, H. a. Gasteiger, M. Piana, S. Catanorchi, Comparative study between platinum supported on carbon and non-noble metal cathode catalyst in alkaline direct ethanol fuel cell (ADEFC), Int. J. Hydrogen Energy. 36 (2011) 5110–5116. doi:10.1016/j.ijhydene.2011.01.079.

[69] A.H.A. Monteverde Videla, D. Sebastian, N.S. Vasile, L. Osmieri, A.S. Aricò, V. Baglio, S. Specchia, Performance analysis of Fe-N-C catalyst for DMFC cathodes: Effect of water saturation in the cathodic catalyst layer, Int. J. Hydrogen Energy. 41 (2016) 22605–22618. doi:10.1016/j.ijhydene.2016.06.060.

[70] K.A. Page, J.W. Shin, S.A. Eastman, B.W. Rowe, S. Kim, A. Kusoglu, K.G. Yager, G.R. Stafford, In Situ Method for Measuring the Mechanical Properties of Nafion Thin Films during Hydration Cycles, ACS Appl. Mater. Interfaces. 7 (2015) 17874–17883. doi:10.1021/acsami.5b04080.

[71] M. Carmo, G. Doubek, R.C. Sekol, M. Linardi, A.D. Taylor, Development and electrochemical studies of membrane electrode assemblies for polymer electrolyte alkaline fuel cells using FAA membrane and ionomer, J. Power Sources. 230 (2013) 169–175.

822 doi:10.1016/j.jpowsour.2012.12.015.
823 [72] P. Piela, C. Eickes, E. Brosha, F. Garzon, P. Zelenay, Ruthenium Crossover in Direct
824 Methanol Fuel Cell with Pt-Ru Black Anode, J. Electrochem. Soc. 151 (2004) A2053–
825 A2059. doi:10.1149/1.1814472.
826 [73] G. Zhang, R. Chenitz, M. Lefèvre, S. Sun, J.P. Dodelet, Is iron involved in the lack of
827 stability of Fe/N/C electrocatalysts used to reduce oxygen at the cathode of PEM fuel cells?,
828 Nano Energy. 29 (2016) 111–125. doi:10.1016/j.nanoen.2016.02.038.
829 [74] H. Wang, Z. Jusys, R.J. Behm, Ethanol electro-oxidation on carbon-supported Pt, PtRu and
830 Pt3Sn catalysts: A quantitative DEMS study, J. Power Sources. 154 (2006) 351–359.
831 doi:10.1007/s10800-006-9174-3.
832 [75] P.A. Christensen, S.W.M. Jones, A. Hamnett, In situ FTIR studies of ethanol oxidation at
833 polycrystalline Pt in alkaline solution, J. Phys. Chem. C. 116 (2012) 24681–24689.
834 doi:10.1021/jp308783y.
835 [76] L. Ma, D. Chu, R. Chen, Comparison of ethanol electro-oxidation on Pt/C and Pd/C catalysts
836 in alkaline media, Int. J. Hydrogen Energy. 37 (2012) 11185–11194.
837 doi:10.1016/j.ijhydene.2012.04.132.
838 [77] C. Busõ-Rogero, E. Herrero, J.M. Feliu, Ethanol oxidation on Pt single-crystal electrodes:
839 Surface-structure effects in alkaline medium, ChemPhysChem. 15 (2014) 2019–2028.
840 doi:10.1002/cphc.201402044.
841 [78] C. Cremers, D. Bayer, B. Kintzel, M. Joos, F. Jung, M. Krausa, J. Tübke, Department,
842 Oxidation of Alcohols in Acidic and Alkaline Environments, ECS Trans. 16 (2008) 1263–
843 1273. doi:10.1149/1.2981967.
844 [79] V. Bambagioni, C. Bianchini, A. Marchionni, J. Filippi, F. Vizza, J. Teddy, P. Serp, M.
845 Zhiani, Pd and Pt-Ru anode electrocatalysts supported on multi-walled carbon nanotubes and
846 their use in passive and active direct alcohol fuel cells with an anion-exchange membrane
847 (alcohol = methanol, ethanol, glycerol), J. Power Sources. 190 (2009) 241–251.

doi:10.1016/j.jpowsour.2009.01.044.

[80] H. Hou, S. Wang, W. Jin, Q. Jiang, L. Sun, L. Jiang, G. Sun, KOH modified Nafion112 membrane for high performance alkaline direct ethanol fuel cell, Int. J. Hydrogen Energy. 36 (2011) 5104–5109. doi:10.1016/j.ijhydene.2010.12.093.

[81] A.D. Modestov, M.R. Tarasevich, A.Y. Leykin, V.Y. Filimonov, MEA for alkaline direct ethanol fuel cell with alkali doped PBI membrane and non-platinum electrodes, J. Power Sources. 188 (2009) 502–506. doi:10.1016/j.jpowsour.2008.11.118.

[82] Y.S. Li, T.S. Zhao, Z.X. Liang, Performance of alkaline electrolyte-membrane-based direct ethanol fuel cells, J. Power Sources. 187 (2009) 387–392. doi:10.1016/j.jpowsour.2008.10.132.

[83] V. Bambagioni, C. Bianchini, Y. Chen, J. Filippi, P. Fornasiero, M. Innocenti, A. Lavacchi, A. Marchionni, W. Oberhauser, F. Vizza, Energy Efficiency Enhancement of Ethanol Electrooxidation on Pd–CeO2/C in Passive and Active Polymer Electrolyte-Membrane Fuel Cells, ChemSusChem. 5 (2012) 1266–1273. doi:10.1002/cssc.201100738.

Highlights

- The ORR kinetics of a Fe-N-C catalyst was investigated using cyclic voltammetry
- Fe-N-C catalyst is more active towards O_2 reduction than H_2O_2 reduction
- Fe-N-C catalyst is ethanol tolerant and shows good durability in RDE
- Performance of alkaline DEFC varies using different ionomer wt. % at cathode
- Short-term DEFC durability was preliminary assessed

Fe-N-C catalysts for ORR

SBA-15 silica

Fe(II) Phthalocyanine

+

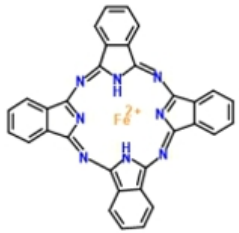

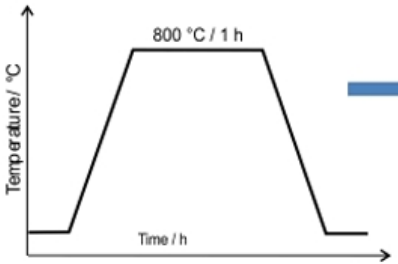

PYROLYSIS

HF

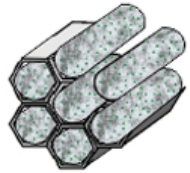

SILICA REMOVAL

Alkaline DEFC